Research Article

Nano Research
2024, 17(6): 4908–4915

ISSN 1998-0124 CN 11-5974/O4
https://doi.org/10.1007/s12274-024-6483-y

Covalent triazine frameworks modified by ultrafine Pt nanoparticles for efficient photocatalytic hydrogen production

Xu Han[1,§], Xueying Ge[3,§], Wen-Wen He[1] (✉), Wangwang Shen[1], Tao Zhou[1], Jian-Sen Wang[2], Rong-Lin Zhong[2] (✉), Abdullah M. Al-Enizi[4], Ayman Nafady[4], and Shengqian Ma[3] (✉)

[1] *School of Chemistry and Life Science, Advanced Institute of Materials Science, Changchun University of Technology, Changchun 130012, China*
[2] *Laboratory of Theoretical and Computational Chemistry, Institute of Theoretical Chemistry, College of Chemistry, Jilin University, Changchun 130021, China*
[3] *Department of Chemistry, University of North Texas, 1508 W. Mulberry St. Denton, TX 76201, USA*
[4] *Department of Chemistry, College of Science, King Saud University, Riyadh 11451, Saudi Arabia*
[§] *Xu Han and Xueying Ge contributed equally to this work.*

Received: 26 October 2023 / **Revised:** 21 December 2023 / **Accepted:** 11 January 2024

ABSTRACT

Pt nanoparticles (PtNPs) as active species have always been considered as one of the best semiconductor materials for photocatalytic hydrogen production. In this study, a Schottky heterojunction has been successfully constructed by evenly loading ultrafine PtNPs onto a triazine-based covalent organic frameworks (COFs). This strategy maintained the high activity of these ultra-small PtNPs while maximizing the utilization of the Pt active sites. The fabricated PtNPs@covalent triazine-based framework-1 (CTF-1) composite accomplished a significantly high rate of hydrogen evolution (20.0 $mmol \cdot g^{-1} \cdot h^{-1}$, apparent quantum efficiency (AQE) = 7.6%, at λ = 450 nm) with 0.40 wt.% Pt loading, giving rise to a 44-fold-increase in the efficiency of the photocatalytic hydrogen production compared to the pristine CTF-1. Theoretical calculations revealed that the strong electron transfer (Q(Pt) = −0.726 q_e, in the analysis of Bader charge, Q(Pt) is the charge quantity transferred from Pt cluster to CTF-1, and q_e is the unit of charge transfer quantity) between PtNPs and CTF-1 triggers a strong interaction, which makes PtNPs being firmly attached to the structure of CTF-1, thereby enabling high stability and excellent hydrogen production efficiency. Importantly, the hydrogen binding free energy (ΔG_{H^*}) of PtNPs@CTF-1 is much lower than that of the unmodified CTF-1, leading to a much lower intermediate state and hence a significant improvement in photocatalytic performance. The overall findings of this work provide a new platform to incorporate metallic NPs into COFs for the design and fabrication of highly efficient photocatalysts.

KEYWORDS

Pt nanoparticles, covalent triazine-based framework-1 (CTF-1), photocatalysts, hydrogen evolution reaction

1 Introduction

Solar energy has been considered as one of the most sustainable, green, and competitive energy sources to resolve the crisis of global energy [1]. In this respect, design and fabrication of high-efficiency photocatalysts is a highly employed approach to boost the utilization of solar energy. In recent years, hydrogen evolution plays a pivotal role in clean energy production to supersede non-renewable resources such as fossil fuels. In particular, metal sulfide, metal oxide, graphitic carbon nitride (g-C_3N_4), metal-organic framework (MOF), and covalent organic framework (COF) as popular semiconductors have been developed to improve the process of hydrogen production [2–4]. Currently, single semiconductor materials evidently have many shortcomings in the field of photocatalytic hydrogen production, such as underutilized active sites, fast recombination of photo-generated electron–hole (e–h) pairs, and poor stability. Hybrid composite materials have been proposed to solve these problems [5, 6].

Due to its low hydrogen evolution overpotential, noble metal platinum (Pt) has always been the preferred co-catalyst for photocatalytic water splitting [7–9]. A direct strategy is to add chloroplatinic acid and semiconductor materials in the testing system, which could greatly promote hydrogen evolution performance under a large amount of Pt. However, in this way, the Pt species usually cannot be recycled [10–13]. In order to enable the recycling of Pt, a strategy of loading platinum nanoparticles (PtNPs) onto semiconductors is favorable. PtNPs can currently be generated from many semi-conducting materials by *in-situ* photodeposition [14]. However, PtNPs synthesized by this method usually have uneven size distribution issues, and are prone to aggregation on the carrier [15]. Therefore, it is very crucial to synthesize non-aggregated PtNPs with a uniform particle size. In doing so, the introduction of polyvinylpyrrolidone (PVP), as a surface capping and reducing agent, can not only prevent the agglomeration of PtNPs, but also make the nanoparticles uniform in size, thus creating more catalytic active sites.

MOFs or two-dimensional (2D) COFs are excellent supports

Address correspondence to Wen-Wen He, heww@ccut.edu.cn; Rong-Lin Zhong, zhongrl898@jlu.edu.cn; Shengqian Ma, Shengqian.Ma@unt.edu

for PtNPs [16, 17]. Compared with MOFs, 2D COFs have better chemical stability and have been widely used as photocatalysts for photocatalytic reactions [18, 19]. Moreover, some advantages of 2D COFs such as favorable pore structures, controllable skeletons, and small band gap make them attractive candidates for photocatalysis [20, 21]. In the design of catalysts, interaction between the carrier and PtNPs can be enhanced by the introduction of N atoms. Meanwhile, the strong interaction between Pt and N atoms can also promote the electron transfer in the photocatalytic reaction [22]. Therefore, we choose covalent triazine-based frameworks (CTFs) as support materials [23]. Constructed by covalent and aromatic triazine bonds, CTFs are similar to graphite materials, having large conjugate systems and high chemical/thermal stability. In particular, preparation process of CTFs is simple and low cost, and these stable CTFs can be reused repeatedly [24, 25]. Adding Pt cocatalyst into the test system can greatly improve the catalytic performance, while modification of CTFs can also improve its photocatalytic capacity. For example, CTF-1 with better crystalline can reach an average H_2 evolution rate of 1.07 mmol·g^{-1}·h^{-1} after *in-situ* photo-deposition of Pt [26]. Pretreating monomers by different acid-base catalysts, Wang et al. obtained a series of CTF-Huazhong University of Science and Technology (HUST) catalysts, and these composites can promote the hydrogen production rate from 2.65 to 9.20 mmol·g^{-1}·h^{-1} using Pt as cocatalyst [27, 28]. Different from monomers pre-modification, the abundant nitrogen source of CTF-1 can also provide active site for guest materials loading. Doping phosphorus on CTF-1 could build a Pt–P–N bond, however, this composite yielded hydrogen evolution rate of 0.61 mmol·g^{-1}·h^{-1} with Pt as cocatalyst [29]. In above-mentioned experiments, Pt co-catalyst was directly added to the photocatalytic test system without adjustment. Compared with the modification schemes focusing on CTFs, strategies based on synthesis and effective loading of ultrafine PtNPs are expected to enhance hydrogen production performance.

Herein, we offer a facile route for the construction of PtNPs@CTF-1 composite, which is anticipated to largely improve the utilization of Pt, thereby achieving efficient hydrogen production. To accomplish this, ultra-small PtNPs were firstly prepared via high temperature nucleation method, followed by loading the as-prepared PtNPs onto black CTF-1 by post decoration method. The formation of this PtNPs@CTF-1 composite can not only evenly disperse PtNPs, but also stabilize the ultra-small PtNPs without aggregation, maintaining the high activity of these ultra-small PtNPs. Thus, the hydrogen evolution rate upon using PtNPs@CTF-1 composite has been boosted greatly with a low Pt loading of 0.40 wt.%, reaching a 20.0 mmol·g^{-1}·h^{-1} (apparent quantum efficiency (AQE) = 7.6%, at λ = 450 nm), which is a 44-fold-incease in the efficiency of the photocatalytic hydrogen production compared with the pristine CTF-1. Practically, the constructed PtNPs@CTF-1 composite has a good stability after passing the hydrogen generation test for four cycles. Additionally, the impedance measurements of PtNPs@CTF-1 have been significantly reduced with marked improvement in the photocurrent. Finally, both X-ray photoelectron spectroscopy (XPS) analysis and density functional theory (DFT) calculations show that there is a strong interaction between PtNPs and CTF-1. Such strong interaction force can make the PtNPs adhere to CTF-1 firmly without falling off. Evidently, the obtained hydrogen binding free energy (ΔG_{H^*}) of PtNPs@CTF-1 is much lower than that of unmodified CTF-1, allowing the hydrogen production process of the composite to have a much lower intermediate state, thereby leading to a significant improvement in photocatalytic performance.

2 Experimental

2.1 Materials

1,4-Dicyanobenzene (DCB), zinc chloride ($ZnCl_2$), sodium hydroxide (NaOH), PVP (molecular weight 10,000), 2,4,5,7-tetrabromofluorescein disodium salt (EY), and chloroplatinic acid hydrate ($H_2PtCl_6·6H_2O$) were purchased from Macklin. Concentrated hydrochloric acid (36%–38%), ethanol, acetone, and triethanolamine (TEOA) were purchased from Greagent. All chemicals were directly used without further purification.

2.2 Synthesis

2.2.1 Synthesis of CTF-1

The synthesis of black CTF-1 was performed by the traditional method (Fig. S1 in the Electroniuc Supplementary Material (ESM)) [23]. The monomer DCB and $ZnCl_2$ were added into the ampere tube at the molar ratio of 1:1. Under the protection of nitrogen, the tube was flame-sealed under vacuum and transferred into the muffle furnace to react at 400 °C for 40 h with a heating rate of 2 °C/min, and finally a black hard block solid was gotten. After grinding, the obtained powder was rinsed with 1 M hydrochloric acid solution for more than 24 h, and then washed with ethanol, acetone, and water successively. Finally, the black powder was obtained by drying overnight in an oven at 80 °C.

2.2.2 Synthesis of PtNPs

The PtNPs were synthesized according to the reported method with some modifications [30, 31]. Typically, 101.5 mg $H_2PtCl_6·6H_2O$ and 142 mg NaOH were added in 20 mL of ethylene glycol in a Schlenk tube. The solution was heated to 160 °C and maintained for 2 h. Before it cooled down completely, 444 mg PVP was thoroughly dissolved in ethanol and added into the dark brown solution. Then the as-synthesized PtNPs were collected by centrifugation at 9000 rpm for 8 min. The sample was then washed with acetone and trichloromethane for three times to remove excess free PVP. The brownish yellow PtNPs were reserved in ethanol for further use.

2.2.3 Synthesis of PtNPs@CTF-1

1, 2, and 3 mL PtNPs ethanol solutions were taken and diluted to 5 mL, respectively. Then 10 mg CTF-1 was added into these PtNPs solutions and stirred for 24 h, separately. Finally, the samples were recovered by suction filtration, and dried overnight at 60 °C. The resulting black solid powder was PtNPs@CTF-1 with different Pt load capacity of 0.33 wt.%, 0.40 wt.%, and 0.44 wt.%. Because of the highest hydrogen production performance, 0.40 wt.% PtNPs@CTF-1 composite was explored as the main material for a series of characterization.

3 Results and discussion

3.1 Structure and characterization of PtNPs@CTF-1

The PtNPs@CTF-1 was synthesized by post modification method in Fig. 1(a). To confirm the composition of the synthesized materials, Fourier transform infrared (FT-IR) spectroscopy and powder X-ray diffraction (PXRD) analysis were undertaken. As shown in Figs. 1(b) and 1(c), the FT-IR spectra and PXRD patterns of CTF-1 are consistent with the ones reported in previous literature, indicating successful synthesis of the black CTF-1. There is no significant change in PXRD diffraction peaks after PtNPs loading, which may be due to the low content of Pt in the composite. In the FT-IR spectra, a weak peak at ~ 2235 cm^{-1}

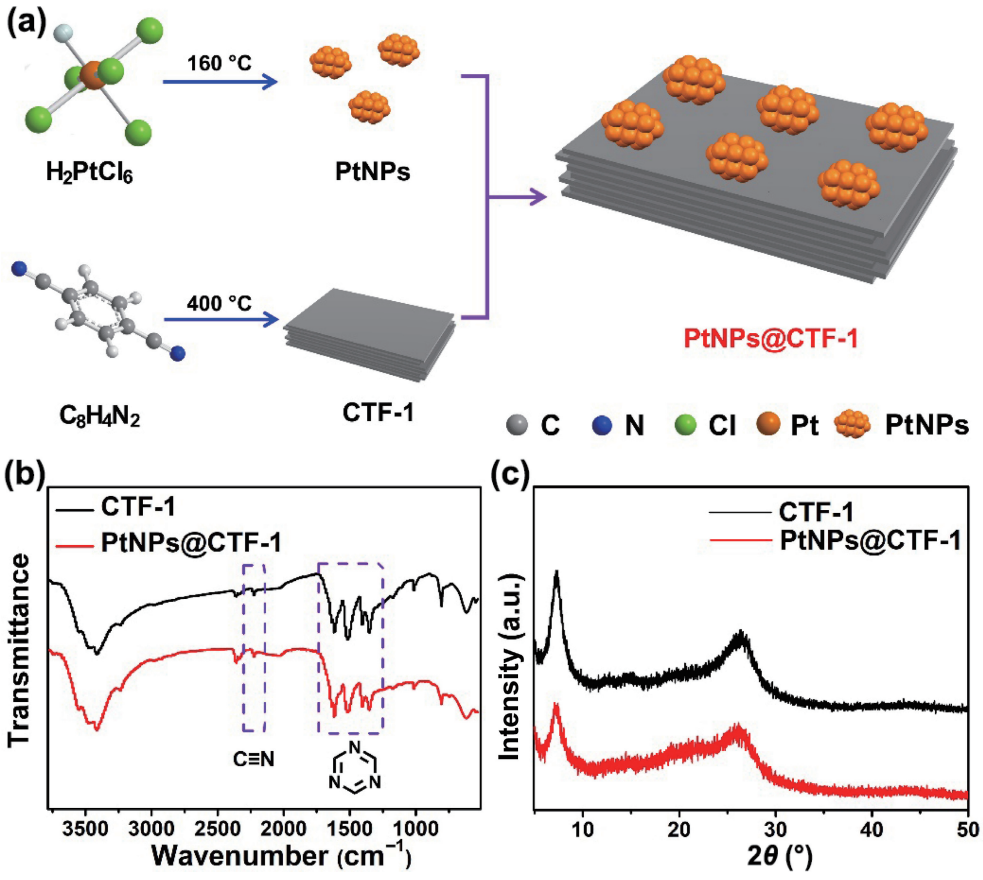

Figure 1 (a) Schematic diagram illustrating the synthesis process of PtNPs@CTF-1 catalyst. (b) FT-IR spectra of CTF-1 and PtNPs@CTF-1. (c) XRD pattern of CTF-1 and PtNPs@CTF-1.

corresponds to –C≡N, whereas the strong peaks at 1510 and 1350 cm^{-1} are attributed to the triazine ring [32]. These peaks indicated that the cyano groups turned into the triazine rings by successful polycondensation. The PXRD patterns of PtNPs@CTF-1 and CTF-1 have two sets of intense XRD peaks. A broad peak appeared at 26.1°, corresponding to an interlayer distance of 3.4 Å for the (001) aromatic ring, while the peaks at 7.3° are assigned to the (100) planes of CTF-1 [21, 22]. Due to the low loading amount and good distribution, the characteristic diffraction peaks of PtNPs in PXRD patterns are not observed. Thermogravimetric analysis (TGA) of the synthesized CTF-1 revealed that the CTF-1 has a good thermal stability (Fig. S2 in the ESM), keeping the skeleton intact without any decomposition until 600 °C. This result matches well with the one reported in previous literatures [33].

In order to probe the morphology of PtNPs on the CTF-1, scanning electron microscopy (SEM) and transmission electron microscopy (TEM) measurements of the composite material (PtNPS@CTF-1) were performed. SEM images revealed that CTF-1 has a flaky structure with a micrometer size (Fig. S3 in the ESM). The mapping spectroscopy images of PtNPs@CTF-1 showed that both C and N elements have been evenly distributed on the composite, whereas the distribution of Pt is almost invisible due to the low content loading. Different from *in-situ* photo-reduction preparation method, PtNPs prepared by high temperature process can reach a smaller size of 1.8 ± 0.2 nm (Figs. 2(a) and 2(b)) and a higher degree of uniformity. As shown in Fig. 2(c), PtNPs are uniformly loaded on CTF-1 without any agglomeration. Such uniform distribution plays a critical role in promoting the exposure of photocatalytic active sites. Meanwhile, the interplanar distance of PtNPs between the neighboring lattice fringes was measured as 0.23 nm (Fig. 2(d)), which was assigned to the (111) lattice plane of the Pt crystals [16, 17]. In addition, the results of inductively coupled plasma-optical emission spectroscopy (ICP-OES) verified that the actual Pt species concentration in PtNPs@CTF-1 is about 0.40 wt.% (Table S1 in the ESM).

XPS is used to study the surface chemical composition and electronic state of the prepared materials. Firstly, all the binding energies of each element were corrected by standard carbon spectrum (C 1s = 284.6 eV). Figure 3(a) shows the wide-scan XPS spectra of CTF-1 and PtNPs@CTF-1, indicating the existence of carbon (C), nitrogen (N), and a small amount of oxygen (O). As shown in Fig. 3(b), the C 1s spectra of CTF-1 and PtNPs@CTF-1 can be deconvoluted into three peaks at 284.3, 285.1, and 286.8 eV, corresponding to sp^2-hybridized carbon (C=C), triazinyl carbon (C=N–C), and the characteristic shake-up line of the aromatic carbon, respectively. After loading PtNPs, the C 1s peak of the composites showed a slight positive shift. In contrast, the XPS characteristic peak of N shows a significant shift to higher binding energy in Fig. 3(c), whose binding energy changed from 398.8 to 399.2 eV, corresponding to triazine N (C=N–C). This is probably due to the existence of an electron flow from N to Pt, giving the high electron density of the catalytic active site. As shown in Fig. 3(d), the high resolution XPS spectrum of Pt 4f was fitted with double peaks for the Pt $4f_{7/2}$ and $4f_{5/2}$. The peaks of pure PtNPs and PtNPs@CTF-1 are at about 71.1 and 74.4 eV, which correspond to the metal Pt^0. Moreover, the peaks of Pt^{2+} are evident at 72.1 and 75.4 eV, which are higher than metallic Pt. Therefore, the valence states of Pt in PtNPs@CTF-1 sample are Pt^{2+} and Pt^0. The above results indicate that there is a strong interaction between PtNPs and CTF-1 [34–36].

3.2 The photocatalytic performance of Pt@CTF-1

After confirming the composition of PtNPs@CTF-1, H_2 generation experiments were performed under visible light (λ >

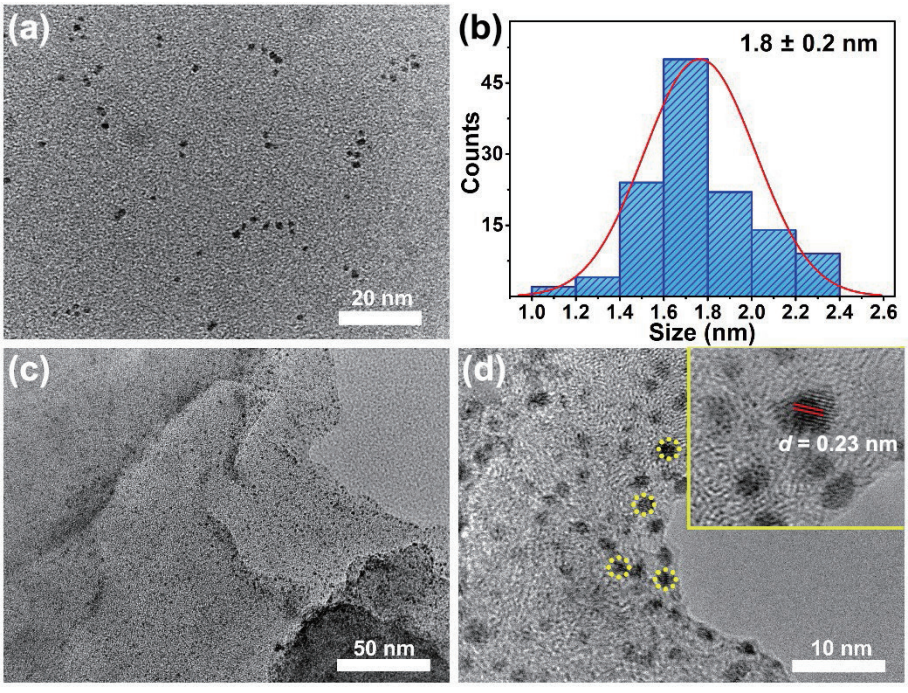

Figure 2 (a) TEM image of PtNPs at the bar of 20 nm. (b) The statistics of particle size distribution. (c) TEM image of PtNPs@CTF-1 at the bar of 50 nm. (d) TEM image of PtNPs@CTF-1 at the bar of 10 nm with the inset of the interplanar distance for PtNPs.

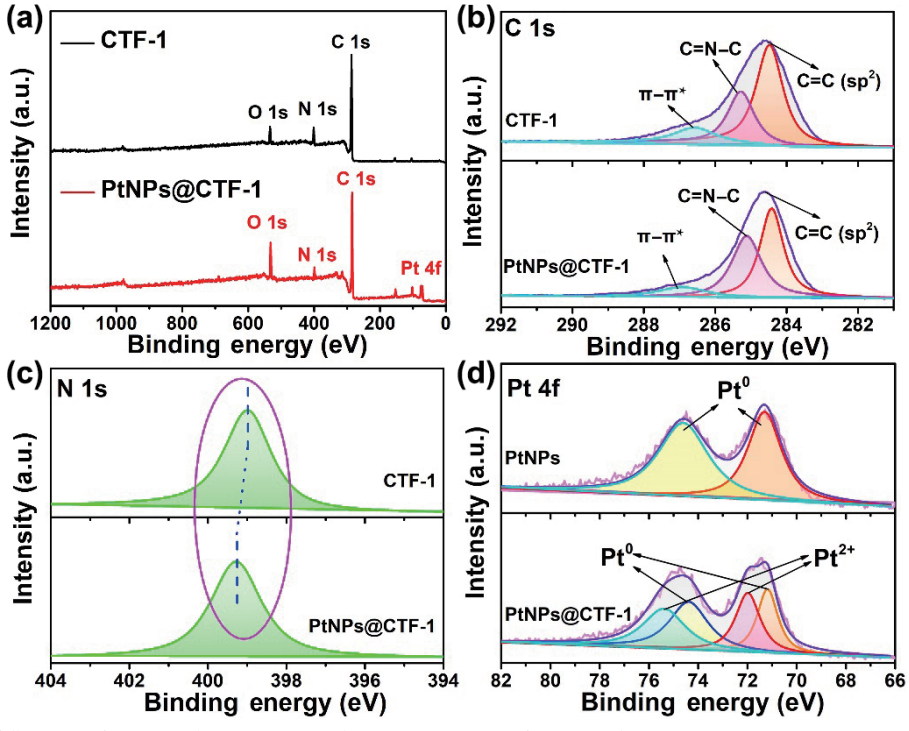

Figure 3 (a) The XPS full spectra of CTF-1 and PtNPs@CTF-1. (b) C 1s XPS spectra of CTF-1 and PtNPs@CTF-1. (c) N 1s XPS spectra of CTF-1 and PtNPs@CTF-1. (d) Pt 4f XPS spectra of PtNPs and PtNPs@CTF-1.

420 nm), with TEOA as the sacrificial electron donor and EY as the photosensitizer (Fig. 4(a) and Fig. S4 in the ESM). The hydrogen evolution rate of CTF-1 is determined to be 0.45 mmol·h^{-1}·g^{-1}. As expected, the deposition of PtNPs onto CTF-1 with 0.4 wt.% Pt content (PtNPs@CTF-1) achieves a maximum hydrogen evolution rate of 20.00 mmol·h^{-1}·g^{-1} (AQE = 7.6%, at λ = 450 nm), which is one of the highest values among the reported photocatalytic systems with Pt as cocatalyst (Table S2 in the ESM). Meanwhile, the H_2 evolution rate of 0.34 wt.% Pt on CTF-1 and 0.44 wt.% Pt on CTF-1 reached 17.00 and 14.92 mmol·h^{-1}·g^{-1}, respectively. This finding demonstrates that 0.40 wt.% Pt content gave the best photocatalytic activity. After four cycles of hydrogen evolution testing, the hydrogen evolution efficiency of PtNPs@CTF-1 catalyst can reach about 83%. Then FT-IR and PXRD were carried out to testify the durability of the composite. The results showed that there are no significant changes in the pattern, proving the high stability of the catalyst (Fig. 4(b) and Fig. S5 in the ESM). Taken together, the combined results clearly establish that the addition of PtNPs has significantly increased the hydrogen evolution rate of CTF-1.

To explore the photocatalytic mechanism of PtNPs@CTF-1, the ultraviolet–visible–diffuse reflectance spectra (UV–vis–DRS) and photoelectrochemical tests were conducted in Fig. 4(c). The UV–vis–DRS spectra of the CTF-1 and PtNPs@CTF-1 have full

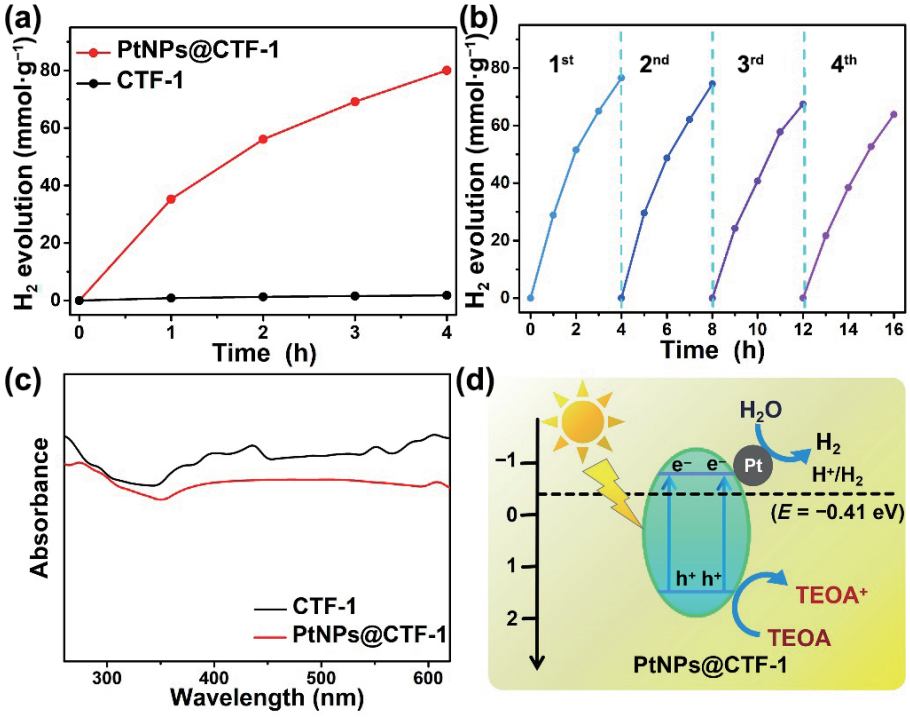

Figure 4 (a) Photocatalytic H_2 evolution rates of pure CTF-1 and PtNPs@CTF-1. (b) Photocatalytic H_2 amount produced by PtNPs@CTF-1 in four consecutive cycles. (c) UV–vis diffuse reflectance spectra of CTF-1 and PtNPs@CTF-1. (d) The reaction mechanism for PtNPs@CTF-1.

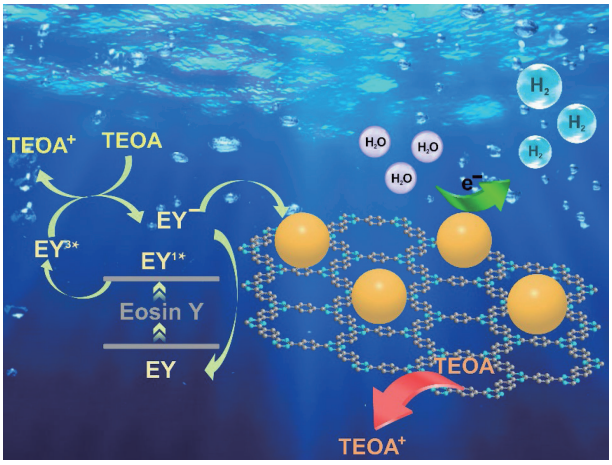

Figure 5 The mechanisms of photocatalytic hydrogen evolution over PtNPs@CTF-1.

absorption in the visible region, which matches the black character of the material [37, 38]. According to the calculation of optical band gaps (Fig. S6 in the ESM), the band gaps values of CTF-1 and PtNPs@CTF-1 are 2.42 and 2.38 eV, respectively. The Mott–Schottky (M–S) measurements (Fig. S7 in the ESM) were performed and the results indicate that PtNPs@CTF-1 and CTF-1 are n-type semiconductors. The calculated flat band potential (V_{FB}) of CTF-1 is −0.82 V vs. Ag/AgCl, which fits the M–S curves of three different frequencies. Upon loading PtNPs, the V_{FB} of PtNPs@CTF-1 changes to −0.94 V vs. Ag/AgCl. The conduction band value (V_{CB}) of PtNPs@CTF-1 is about −0.74 V vs. normal hydrogen electrode (NHE), whereas the potential of the valence band value (V_{VB}) of PtNPs@CTF-1 is 1.64 V vs. NHE, based on the band gap results (pH = 7). It can be seen from these results that PtNPs@CTF-1 has a suitable band gap structure for H_2 evolution reaction from H_2O (Fig. 4(d)).

In conclusion, the hydrogen production mechanism of PtNPs@CTF-1 can be summarized as follows: When the PtNPs@CTF-1 composite is irradiated by visible light, the semiconductor CTF-1 is excited to generate e–h pairs, where the electrons transfer to conduction band and the holes stay on the valence band of CTF-1. Simultaneously, the ground state of EY absorbs photoelectrons, converting to the singlet excited state EY^{1*}. Through the intersystem transition, it converts to a more stable triplet excited state EY^{3*}. While the TEOA molecules with strong reducing ability accessed into the solution, occupying the hole of the CTF-1 and preventing the photo-induced electrons from moving to the valence band of CTF-1 around hydrogen production. Meanwhile, the TEOA is oxidized to $TEOA^+$ thereby assisting EY^{3*} to convert into EY^- [39, 40]. Then, the electrons from these processes will transfer to the PtNPs to combine with H_2O, leading to the formation of H_2 (Fig. 5).

Photoluminescence (PL) spectra (Figs. 6(a) and 6(b)) were used to verify the separation ability of photoelectron–hole pairs. Under the excitation of 380 nm, a strong emission peak at 554 nm caused by the EY is presented. When the CTF-1 is added to the test solution, the altitude of emission peak is slightly weakened. Upon adding PtNPs@CTF-1, the emission peak changes evidently, which is caused by the sluggish recombination of photogenerated electrons and holes. The electrochemical impedance spectroscopy (EIS) and photocurrent response (Figs. 6(c) and 6(d)) were used to further verify the in-depth photophysical mechanism. It follows that the semicircle of Nyquist curve of PtNPs@CTF-1 is extremely smaller than CTF-1 under the visible light, indicating that the impedance of the composite has been greatly reduced and the kinetics performance of the composite has been significantly improved. The overall results clearly indicate that PtNPs@CTF-1 is more conducive for electron transfer. Whereas the photocurrent results implied that the light-response ability is obviously improved after loading of PtNPs, reflecting that the composite material has good photo-response abilities.

3.3 The DFT theoretical calculation of PtNPs@CTF-1

To further explore the interaction between PtNPs and CTF-1 along with the study of the dynamic mechanism of the photocatalytic hydrogen evolution reaction (HER), dynamic simulations and DFT calculations were performed. After optimization (Fig. 7 and Fig. S8 in the ESM), the maximum

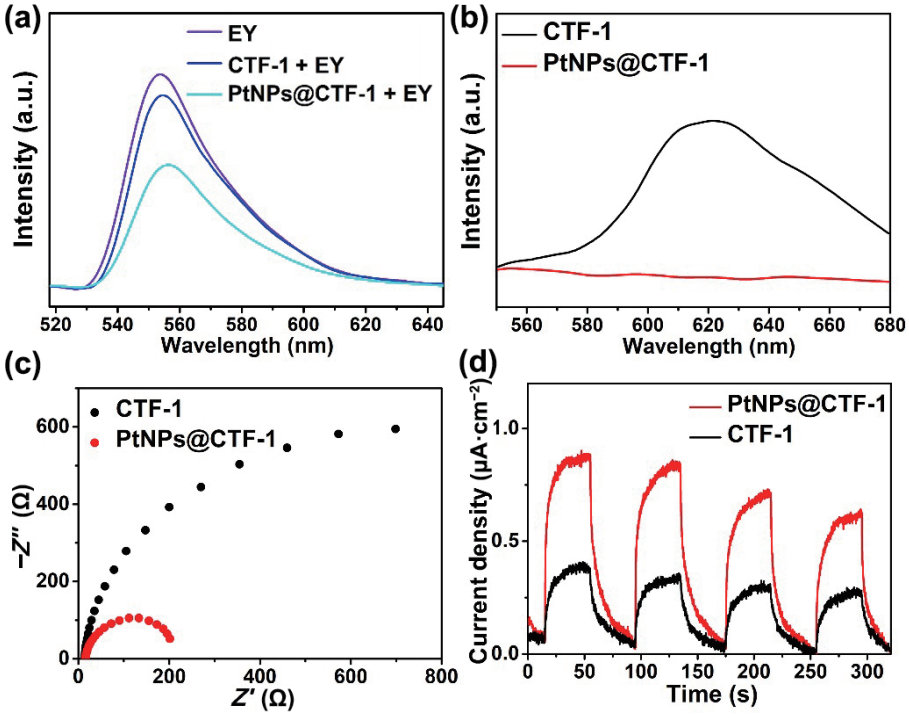

Figure 6 (a) PL spectra with EY. (b) Steady-state PL spectra without EY of CTF-1 and PtNPs@CTF-1. (c) EIS curves of CTF-1 and PtNPs@CTF-1. (d) Transient photocurrent responses of CTF-1 and PtNPs@CTF-1 (under the xenon lamp, $\lambda > 420$ nm).

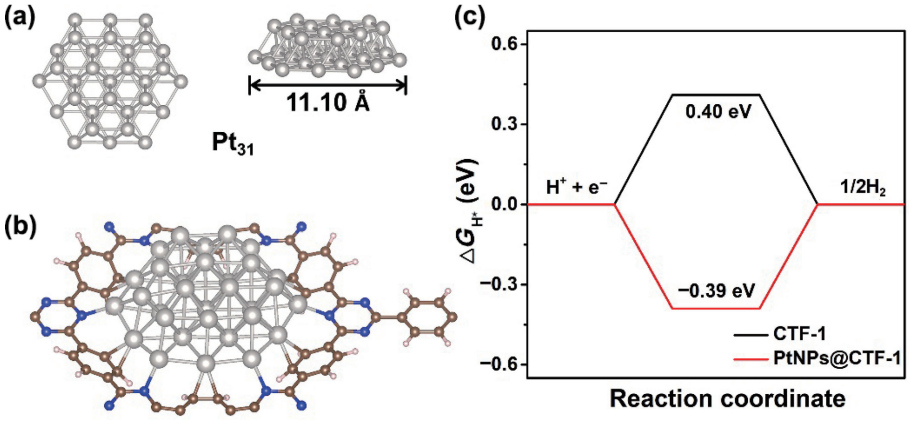

Figure 7 (a) Geometry structures for Pt_{31} NPs (the left image is the upward view, and the right image is the front view). (b) Geometry structures for Pt_{31}@CTF-1. (c) Calculated free energy of PtNPs@CTF-1 for the photocatalytic H_2 evolution.

distance between the two nitrogen atoms in the channel of CTF-1 is 14.60 Å (Fig. S8(a) in the ESM). Based on this, the configuration of PtNPs@CTF-1 is built with the Pt_{31} in the way of double-layer superposition (Figs. 7(a) and 7(b)). From the results of the Bader charge distribution (Fig. S8(c) in the ESM), it can be concluded that there is a strong charge interaction (Q(Pt) = −0.726 q_e, in the analysis of Bader charge, Q(Pt) is the charge quantity transferred from Pt cluster to CTF-1, and q_e is the unit of charge transfer quantity) between the nanoparticles and carrier, which may be the reason why PtNPs can be firmly fixed on CTF-1. With regard to the electron distribution between N and Pt, it exhibits significant depletion of electrons on N atom, thus might manifest the transfer of electrons from N atom to Pt. It is consistent with the XPS results. Taken together, all the aforementioned results indicate that the strong interaction between PtNPs and CTF-1 may provide a good stability of the composite.

To understand the difficulty of hydrogen evolution reaction, ΔG_{H^*} is calculated (Fig. 7(c) and Fig. S9 in the ESM). The ΔG_{H^*} of CTF-1 and PtNPs@CTF-1 is 0.41 and −0.39 eV, suggesting that the intermediate state of PtNPs@CTF-1 is lower in energy, which is highly favored for hydrogen evolution reaction process. In view of the obtained results, it can be concluded that good durability of the PtNPs@CTF-1 catalyst may be attributed to the electron donation process occurring between PtNPs and CTF-1. Meanwhile, the photocatalytic HER of water by PtNPs@CTF-1 is thermodynamically favorable.

4 Conclusions

In summary, a hybrid material comprising PtNPs@CTF-1 has been successfully fabricated with the characteristics of having efficient visible light response, suitable band gap matching, and effective e–h separation ability for photocatalytic hydrogen production via water splitting. The results showed that PtNPs@CTF-1 with a loading capacity of 0.40 wt.% Pt gave rise to a hydrogen production rate of 20.0 mmol·g^{-1}·h^{-1} (AQE = 7.6%, at λ = 450 nm), which is much higher than pure CTF-1 and other related hybrid materials. According to the result of XPS and DFT, the electron transfer (Q(Pt) = −0.726 q_e) between PtNPs and CTF-1 triggers a strong interaction, which makes PtNPs being firmly anchored to the structure of CTF-1, giving the composite very good stability and excellent hydrogen production capacity. Subsequently, the results of ΔG_{H^*} are certified that the

PtNPs@CTF-1 composite material gave the hydrogen production process a much lower intermediate state, thereby leading to a significant improvement in photocatalytic performance. This work proposes a novel strategy for combining metallic nanoparticles with CTFs for the construction of highly efficient photocatalytic hydrogen production catalysts, facilitating the design of other PtNPs/COFs hybrid materials for photocatalytic applications.

Acknowledgements

This work was financially supported by the National Natural Science Foundation of China (Nos. 22271022 and 21701016) and the Science and Technology Development Planning of Jilin Province (No. YDZJ202201ZYTS342). This paper was also supported by the China Scholarship Council (CSC No. 201802335014). Partial support from the Robert A. Welch Foundation (B-0027) (S.M.) and Researchers Supporting Program (No. RSP-2024R55) at King Saud University, Riyadh, Saudi Arabia is also acknowledged.

Electronic Supplementary Material: Supplementary material (characterization, photocatalytic activity test, calculation of AQE, TGA spectra, SEM-energy-dispersive X-ray (EDX) analysis, FT-IR spectra, XRD pattern electrochemical and optical properties, and geometric optimization calculations) is available in the online version of this article at https://doi.org/10.1007/s12274-024-6483-y.

References

[1] Li, W.; Elzatahry, A.; Aldhayan, D.; Zhao, D. Y. Core–shell structured titanium dioxide nanomaterials for solar energy utilization. *Chem. Soc. Rev.* **2018**, *47*, 8203–8237.

[2] Kumar, A.; Krishnan, V. Vacancy engineering in semiconductor photocatalysts: Implications in hydrogen evolution and nitrogen fixation applications. *Adv. Funct. Mater.* **2021**, *31*, 2009807.

[3] Yasuda, M.; Matsumoto, T.; Yamashita, T. Sacrificial hydrogen production over TiO_2-based photocatalysts: Polyols, carboxylic acids, and saccharides. *Renew. Sustain. Energy Rev.* **2018**, *81*, 1627–1635.

[4] Yin, L. Y.; Zhao, Y. N.; Xing, Y. M.; Tan, H. Q.; Lang, Z. L.; Ho, W.; Wang, Y. H.; Li, Y. G. Structure–property relationship in β-keto-enamine-based covalent organic frameworks for highly efficient photocatalytic hydrogen production. *Chem. Eng. J.* **2021**, *419*, 129984.

[5] Wang, Z.; Li, C.; Domen, K. Recent developments in heterogeneous photocatalysts for solar-driven overall water splitting. *Chem. Soc. Rev.* **2019**, *48*, 2109–2125.

[6] Li, Z.; Zi, J. Z.; Luan, X.; Zhong, Y. Q.; Qu, M. H.; Wang, Y. Z.; Lian, Z. C. Localized surface plasmon resonance promotes metal-organic framework-based photocatalytic hydrogen evolution. *Adv. Funct. Mater.* **2023**, *33*, 2303069.

[7] Dao, D. Q.; Anh Nguyen, T. K.; Kang, S. G.; Shin, E. W. Engineering oxidation states of a platinum cocatalyst over chemically oxidized graphitic carbon nitride photocatalysts for photocatalytic hydrogen evolution. *ACS Sustain. Chem. Eng.* **2021**, *9*, 14537–14549.

[8] Sun, L. L.; Han, L.; Huang, J. T.; Luo, X. D.; Li, X. B. Single-atom catalysts for photocatalytic hydrogen evolution: A review. *Int. J. Hydrogen Energy* **2022**, *47*, 17583–17599.

[9] Aggarwal, P.; Sarkar, D.; Awasthi, K.; Menezes, P. W. Functional role of single-atom catalysts in electrocatalytic hydrogen evolution: Current developments and future challenges. *Coord. Chem. Rev.* **2022**, *452*, 214289.

[10] Mohammadnezhad, F.; Kampouri, S.; Wolff, S. K.; Xu, Y. K.; Feyzi, M.; Lee, J. H.; Ji, X. L.; Stylianou, K. C. Tuning the optoelectronic properties of hybrid functionalized MIL-125-NH_2 for photocatalytic hydrogen evolution. *ACS Appl. Mater. Interfaces* **2021**, *13*, 5044–5051.

[11] Zhang, F. M.; Sheng, J. L.; Yang, Z. D.; Sun, X. J.; Tang, H. L.; Lu, M.; Dong, H.; Shen, F. C.; Liu, J.; Lan, Y. Q. Rational design of MOF/COF hybrid materials for photocatalytic H_2 evolution in the presence of sacrificial electron donors. *Angew. Chem., Int. Ed.* **2018**, *57*, 12106–12110.

[12] Li, C. Z.; Liu, J. L.; Li, H.; Wu, K. F.; Wang, J. H.; Yang, Q. H. Covalent organic frameworks with high quantum efficiency in sacrificial photocatalytic hydrogen evolution. *Nat. Commun.* **2022**, *13*, 2357.

[13] Wei, S. C.; Zhang, F.; Zhang, W. B.; Qiang, P. R.; Yu, K. J.; Fu, X. B.; Wu, D. Q.; Bi, S.; Zhang, F. Semiconducting 2D triazine-cored covalent organic frameworks with unsubstituted olefin linkages. *J. Am. Chem. Soc.* **2019**, *141*, 14272–14279.

[14] Moon, H. S.; Hsiao, K. C.; Wu, M. C.; Yun, Y. J.; Hsu, Y. J.; Yong, K. Spatial separation of cocatalysts on Z-scheme organic/inorganic heterostructure hollow spheres for enhanced photocatalytic H_2 evolution and in-depth analysis of the charge-transfer mechanism. *Adv. Mater.* **2023**, *35*, 2200172.

[15] Xu, M. L.; Li, D. D.; Sun, K.; Jiao, L.; Xie, C. F.; Ding, C. M.; Jiang, H. L. Interfacial microenvironment modulation boosting electron transfer between metal nanoparticles and MOFs for enhanced photocatalysis. *Angew. Chem., Int. Ed.* **2021**, *60*, 16372–16376.

[16] Nguyen, H. L. Metal-organic frameworks can photocatalytically split water-why not. *Adv. Mater.* **2022**, *34*, 2200465.

[17] Mi, Z.; Zhou, T.; Weng, W. J.; Unruangsri, J.; Hu, K.; Yang, W. L.; Wang, C. C.; Zhang, K. A. I.; Guo, J. Covalent organic frameworks enabling site isolation of viologen-derived electron-transfer mediators for stable photocatalytic hydrogen evolution. *Angew. Chem., Int. Ed.* **2021**, *60*, 9642–9649.

[18] Liu, S. Z.; Guo, Z.; Qian, X. H.; Zhang, J. Y.; Liu, J. X.; Lin, J. Sonochemical deposition of ultrafine metallic Pt nanoparticles on CdS for efficient photocatalytic hydrogen evolution. *Sustain. Energy Fuels* **2019**, *3*, 1048–1054.

[19] Wang, H.; Wang, H.; Wang, Z. W.; Tang, L.; Zeng, G. M.; Xu, P.; Chen, M.; Xiong, T.; Zhou, C. Y.; Li, X. Y. et al. Covalent organic framework photocatalysts: Structures and applications. *Chem. Soc. Rev.* **2020**, *49*, 4135–4165.

[20] Wang, T. N.; Azhar, I.; Yang, Y. T.; Lu, Y.; Tian, Y. Y.; Gao, N.; Cui, F. C.; Yang, L.; Jing, X. F.; Zhu, G. S. Fine-tuned mesoporous covalent organic frameworks for highly efficient low molecular-weight proteins separation. *Nano Res.* **2022**, *15*, 4569–4574.

[21] Liu, Y. N.; Jiang, L. C.; Tian, Y. Y.; Xu, Z. F.; Wang, W. T.; Qiu, M.; Wang, H. M.; Li, X.; Zhu, G. S.; Wang, Y. G. Covalent organic framework/g-C_3N_4 van der Waals heterojunction toward H_2 production. *Inorg. Chem.* **2023**, *62*, 3271–3277.

[22] Hu, Y. D.; Qu, Y. T.; Zhou, Y. S.; Wang, Z. Y.; Wang, H. J.; Yang, B.; Yu, Z. Q.; Wu, Y. E. Single Pt atom-anchored C_3N_4: A bridging Pt–N bond boosted electron transfer for highly efficient photocatalytic H_2 generation. *Chem. Eng. J.* **2021**, *412*, 128749.

[23] Kuhn, P.; Antonietti, M.; Thomas, A. Porous, covalent triazine-based frameworks prepared by ionothermal synthesis. *Angew. Chem., Int. Ed.* **2008**, *47*, 3450–3453.

[24] Hasija, V.; Patial, S.; Raizada, P.; Aslam Parwaz Khan, A.; Asiri, A. M.; Van Le, Q.; Nguyen, V. H.; Singh, P. Covalent organic frameworks promoted single metal atom catalysis: Strategies and applications. *Coord. Chem. Rev.* **2022**, *452*, 214298.

[25] Lan, Z. A.; Wu, M.; Fang, Z. P.; Zhang, Y. F.; Chen, X.; Zhang, G. G.; Wang, X. C. Ionothermal synthesis of covalent triazine frameworks in a NaCl-KCl-$ZnCl_2$ eutectic salt for the hydrogen evolution reaction. *Angew. Chem.* **2022**, *134*, e202201482.

[26] Kuecken, S.; Acharjya, A.; Zhi, L. J.; Schwarze, M.; Schomäcker, R.; Thomas, A. Fast tuning of covalent triazine frameworks for photocatalytic hydrogen evolution. *Chem. Commun.* **2017**, *53*, 5854–5857.

[27] Wang, K. W.; Yang, L. M.; Wang, X.; Guo, L. P.; Cheng, G.; Zhang, C.; Jin, S. B.; Tan, B. E.; Cooper, A. Covalent triazine frameworks via a low-temperature polycondensation approach. *Angew. Chem., Int. Ed.* **2017**, *56*, 14149–14153.

[28] Zhang, S. Q.; Cheng, G.; Guo, L. P.; Wang, N.; Tan, B. E.; Jin, S. B. Strong-base-assisted synthesis of a crystalline covalent triazine

framework with high hydrophilicity via benzylamine monomer for photocatalytic water splitting. *Angew. Chem., Int. Ed.* **2020**, *59*, 6007–6014.

[29] Zheng, L. L.; Wang, D. K.; Wu, S. L.; Jiang, X. H.; Zhang, J.; Xing, Q. J.; Zou, J. P.; Luo, S. L. Unveiling localized Pt–P–N bonding states constructed on covalent triazine-based frameworks for boosting photocatalytic hydrogen evolution. *J. Mater. Chem. A* **2020**, *8*, 25425–25430.

[30] Wang, X.; Zhuang, J.; Peng, Q.; Li, Y. D. A general strategy for nanocrystal synthesis. *Nature* **2005**, *437*, 121–124.

[31] Liu, W.; Wang, H. L. Influence of surface capping on oxygen reduction catalysis: A case study of 1.7 nm Pt nanoparticles. *Surf. Sci.* **2016**, *648*, 120–125.

[32] Li, S. Y.; Li, W. H.; Wu, X. L.; Tian, Y. Y.; Yue, J. Y.; Zhu, G. S. Pore-size dominated electrochemical properties of covalent triazine frameworks as anode materials for K-ion batteries. *Chem. Sci.* **2019**, *10*, 7695–7701.

[33] Kong, D.; Han, X. Y.; Xie, J. J.; Ruan, Q. S.; Windle, C. D.; Gadipelli, S.; Shen, K.; Bai, Z. M.; Guo, Z. X.; Tang, J. W. Tunable covalent triazine-based frameworks (CTF-0) for visible-light-driven hydrogen and oxygen generation from water splitting. *ACS Catal.* **2019**, *9*, 7697–7707.

[34] Zhao, M. T.; Yuan, K.; Wang, Y.; Li, G. D.; Guo, J.; Gu, L.; Hu, W. P.; Zhao, H. J.; Tang, Z. Y. Metal-organic frameworks as selectivity regulators for hydrogenation reactions. *Nature* **2016**, *539*, 76–80.

[35] Xu, N. Z.; Liu, Y. B.; Yang, W. J.; Tang, J.; Cai, B. W.; Li, Q.; Sun, J. W.; Wang, K. Q.; Xu, B. L.; Zhang, Q. T. et al. 2D–2D heterojunctions of a covalent triazine framework with a triphenylphosphine-based covalent organic framework for efficient photocatalytic hydrogen evolution. *ACS Appl. Energy Mater.* **2020**, *3*, 11939–11946

[36] Huang, H. M.; Xu, B.; Tan, Z. K.; Jiang, Q. Q.; Fang, S. Q.; Li, L. Y.; Bi, J. H.; Wu, L. A facile *in situ* growth of CdS quantum dots on covalent triazine-based frameworks for photocatalytic H_2 production. *J. Alloys Compd.* **2020**, *833*, 155057.

[37] Ma, X. H.; Liu, Y. N.; Wang, Y. P.; Jin, Z. L. Co_3O_4/CeO_2 p–n heterojunction construction and application for efficient photocatalytic hydrogen evolution. *Int. J. Hydrogen Energy* **2021**, *46*, 33809–33822.

[38] Xie, J. J.; Shevlin, S. A.; Ruan, Q. S.; Moniz, S. J. A.; Liu, Y. R.; Liu, X.; Li, Y. M.; Lau, C. C.; Guo, Z. X.; Tang, J. W. Efficient visible light-driven water oxidation and proton reduction by an ordered covalent triazine-based framework. *Energy Environ. Sci.* **2018**, *11*, 1617–1624.

[39] Zhen, W. L.; Gao, H. B.; Tian, B.; Ma, J. T.; Lu, G. X. Fabrication of low adsorption energy Ni-Mo cluster cocatalyst in metal-organic frameworks for visible photocatalytic hydrogen evolution. *ACS Appl. Mater. Interfaces* **2016**, *8*, 10808–10819.

[40] Yang, L. Q.; Huang, J. F.; Shi, L.; Cao, L. Y.; Zhou, W.; Chang, K.; Meng, X. G.; Liu, G. G.; Jie, Y. N.; Ye, J. H. Efficient hydrogen evolution over Sb doped SnO_2 photocatalyst sensitized by Eosin Y under visible light irradiation. *Nano Energy* **2017**, *36*, 331–340.